UNIVERSIDADE DE SÃO PAULO

INSTITUTO DE FÍSICA
CAIXA POSTAL 20516
01000 - SÃO PAULO - SP
BRASIL

publicações

IFUSP/P-381

THE $^{12}C(d,n)^{13}N$ REACTION BETWEEN $E_d = 7.0$ AND 13.0 MeV

by

H.R. Schelin, E. Farrelly Pessoa, W.R. Wylie, E.W. Cybulska, K. Nakayama and L.M. Fagundes

Departamento de Física Nuclear, Instituto de Física, Universidade de São Paulo

and

R.A. Douglas

Depto. de Física Aplicada, IFGW, Universidade Estadual de Campinas, São Paulo, Brasil

Dezembro/1982

THE $^{12}C(d,n)^{13}N$ REACTION BETWEEN E_d=7.0 AND 13.0 MeV

H.R. Schelin*, E. Farrelly Pessoa, W.R. Wylie*,
E.W. Cybulska, K. Nakayama and L.M. Fagundes

Departamento de Física Nuclear, Instituto de Física,
Universidade de São Paulo, São Paulo, Brasil.

and

R.A. Douglas

Departamento de Física Aplicada, IFGW,
Universidade Estadual de Campinas, São Paulo, Brasil.

ABSTRACT

Absolute differential cross sections for the n_o , n_1 and (n_2+n_3) neutron groups from the reaction $^{12}C(d,n)^{13}N$ have been measured at incident deuteron energies of 7.0 , 9.1 and 13.0 MeV along with an excitation curve at $\theta_{lab} = 25^o$ from E_d = 10.6 to 13.0 MeV. Analysis of energy averaged cross sections included distorted wave Born approximation (DWBA) calculations and Hauser Feshbach statistical model calculations. Direct interaction and Hauser Feshbach reduction factors are obtained and compared to previously reported values.

NUCLEAR REACTIONS $^{12}C(d,n)^{13}N$, E_d = 7.0, 9.1 and 13.0 MeV; measured $\sigma(E_d,\theta)$. Excitation function at $\theta_{lab} = 25^o$ for E_d = 10.6 to 13.0 MeV. Direct interaction and Hauser Feshbach reduction factors deduced. Time of-flight neutron detection.

*Present address:- Centro Técnico Aerospacial, IEAv/FEX,
Caixa Postal
12200 São José dos Campos, São Paulo, Brasil.

1. INTRODUCTION

The (d,n) stripping process for p-shell nuclei is accompanied by compound nucleus formation which may persist up to rather high incident deuteron energies. Although the direct interaction dominates the angular distributions of the emergent neutrons at the forward scattering angles, an appreciable amount of the neutrons detected at more backward angles may result from the decay of the compound nucleus. Thus a proper analysis should take these two reaction mechanisms into account. Hodgson (Ho 71) has shown that by using energy averaged differential cross sections, it is possible to add the contributions of the two reaction mechanisms incoherently. The present work is a study of the $^{12}C(d,n)^{13}N$ reaction between E_d = 7.0 and 13.0 MeV for the purpose of determining the relative contributions of the reaction mechanisms and thus the spectroscopic factors for the low lying states in ^{13}N .

Various measurements have been made for the $^{12}C(d,n)^{13}N$ reaction. Gangadharen and Wolke (Ga 70), using a ^{13}N recoil detector measured the value 0.68 mb/sr for the n_o cross section at E_d = 12 MeV and $\theta_{cm} = 30^o$. For this same cross section at 11.8 MeV Mutchler et al. (Mu 71) using time-of-flight techniques measured the value 6.4 mb/sr. Davis and Din (Da 72) used a stilbene neutron detector to measure the n_o excitation function at $\theta=0^o$ in the energy range E_d = 3.6 to 12.0 MeV. At E_d = 11.8 MeV their differential cross section is of the order of 36 mb/sr as compared to the Mutcher et al. results, extrapolated to 0^o, of about 15-20 mb/sr. More recently Shirato (Sh 81) used deuteron beam stopping techniques to measure the 0^o excitation function in the region E_d = = 7-10 MeV. Although he found a similarity in structure with

the Davis and Din curve, his cross sections are about one third their magnitude.

The reported spectroscopic values also show some disagreement. For the ground state of ^{13}N , Davis and Din (Da 72) report a value S = 0.73 which was obtained from an energy averaged angular distribution at 8.0 MeV whose analysis included both DWBA and Hauser Feshbach contributions. For this same state, Mutchler et al. (Mu 71) extracted the value S=0.74 from an angular distribution at 11.8 MeV, which, while agreeing well with the Davis and Di value, was obtained with no account taken of compound nucleus contributions to the cross section and a normalization which depended exclusively on the forward scattering angle data. Azimov et al. (Az 75) obtained the value S=0.38 for this state from an angular distribution at E_d = 15.25 MeV where again no inclusion of Hauser Feshbach predictions was made.

For the first excited state of ^{13}N , Mutchler et al. (Mu 71) reported a spectroscopic factor S=1.02 which is much higher than the value reported by Fortune et al. (Fo 69) of S=0.25 obtained from the $^{12}C(\tau,d)^{13}N$ reaction.

In view of the situation we decided to measure two angular distributions at 7.0 MeV and 9.1 MeV in order to obtain an energy averaged differential cross section at 8.0 MeV and a third angular distribution at E_d = 13.0 MeV which together with the Mutchler angular distribution at 11.8 MeV provided us with an energy averaged differential cross section at 12.4 MeV. In addition, an excitation curve at $\theta_{lab} = 25^o$ was measured in 200 keV steps in the interval E_d = 10.6 to 13.0 MeV. The Mutchler data was normalized to this excitation curve.

An analysis of the energy averaged cross sections included both the DWBA stripping contribution and the Hauser Feshbach compound nucleus contribution. Spectroscopic factors are reported for both the ground state and first excited state in ^{13}N along with the Hauser Feshbach reduction factors employed in the analyses.

2. EXPERIMENTAL PROCEDURE

2.1. The Beam and the Target Chamber

The University of São Paulo Tandem Pelletron provided pulsed and klystron bunched deuteron beams between 7.0 and 13.0 MeV. The time averaged on-target beam intensity was 50 nanoamps. The time resolution of the system, obtained from the FWHM of the target gamma ray peak, was 1.5 ns. A detailed description of the pulsing system may be found in (Wy 79).

A low mass stainless steel scattering chamber of diameter 22 cm and height 12 cm with 1 mm walls was used in order to minimize neutron absorption and scattering. The chamber has four target holders each of which may be alligned with the beam without disturbing the vacuum.

The beam was collimated 7 cm ahead of the target by a 5 mm diameter tantalum aperture. The ratio of collimator to target current was maintained less than 1:50. The beam was stopped 1.5 meters beyond the target in an electrically and magnetically suppressed Faraday cup located at the center of a water-filled, 40 cm long cubical box with 5 cm lead walls.

2.2. The Neutron Detector

Neutrons were detected in a 12.7 cm diameter × × 5 cm thick Nuclear Enterprise NE213 liquid scintillator optically coupled to a RTC58AVP photomultiplier. The photomultiplier was mounted on an ORTEC model 271 base and the unit was wrapped in netic and conetic magnetic shielding and enclosed in a 5 cm thick lead housing. This entire unit was surrounded by a 39 cm diameter by 77 cm long borax loaded paraffin cylindrical shield mounted on a remote controlled cart and tracks which allowed a maximum flight path of 6 meters. A bore through the paraffin shield which extended 45 cm from the shield entrance to the face of the scintillator was lined with an iron tube with 1.8 cm thick walls. As seen in fig.1 these precautions reduced the uncorrelated background in the neutron spectra to a negligible amount.

The detection efficiency of the NE 213 scintillator was calculated from a Monte Carlo computer code (Na 81) which requires as input the gamma ray energy corresponding to the minimum electron pulse height accepted for analysis. This pulse height bias level was equivalent to about 10 times the 60 keV total absorption peak from an ^{241}Am source and was repeatedly measured during the experiment.

2.3. The Time-of-Flight System

A block diagram of the electronic arrangement used to obtain the neutron time-of-flight spectra is shown in fig.2. The neutron groups from the (d,n) reaction are analysed by the time-to-amplitude converter (TAC 1) operating with a 400 ns ramp. The photomultiplier anode pulse triggers the constant

fraction discriminator (CFD) in the base module which starts the ramp. The stop signal is taken from the master oscillator which controls the beam pulsing system. The time calibration of TAC 1 (0.345ns/ch) was obtained with a Tektronics time-mark generator.

The n/γ discrimination circuit uses risetime selection with an ORTEC model 455 timing single channel analyser (TSCA) to distinguish between the rise times caused by neutrons and gammas in the scintillator. Pulses from dynode 9 of the PM are sent to the TSCA operated in the integral mode. The lower level of this TSCA determined the neutron pulseheight threshold used in the efficiency calculation. The output of the TSCA starts TAC 2. The stop signals for TAC 2 which are independent of risetime are obtained from the PM anode after passage through a constant fraction discrimiator CFD. With this circuit the efficiency for gamma ray detection was decreased by 90% without diminishing the neutron detection efficiency.

The outputs of the TAC's and the linear amplifiers go to an ADC bank and a Honeywell DDP516 on-line computer which allows display of the various spectra and storage on magnetic tape through a link to an IBM 360/44 computer.

2.3. The Monitor

A small NE111 plastic scintillator coupled to an RCA 8575 phototube was mounted near the target at 90° to the beam direction, as a monitor of target condition and time calibration. The neutron threshold of the monitor was set at about 7 MeV. The shape and positions of the target gamma ray and ground state neutron peak were checked periodically.

2.4. The Targets

The ^{12}C targets consisted of self supporting films of polystyrene. The target thickness and uniformity were determined by measuring the energy loss of ^{241}Am alpha particles in the target material. The number of ^{12}C nuclei/cm^2, N, was calculated from the following formula

$$N = \frac{t \times n' \times A}{M} \qquad (1)$$

where t is the target thickness in g/cm^2, n' is the number of ^{12}C nuclei per polystyrene molecule, A is Avogado's number and M is the gram molecular weight of polystyrene. Table 1 is a resumé of the characteristics of the targets used in the present work.

3. THE DATA REDUCTION

Figure 1 shows a typical neutron time-of-flight spectrum for the reaction $^{12}C(d,n)^{13}N$ obtained for $\theta_{lab} = 30^{\circ}$ and $E_d = 9.1$ MeV. Three prominent peaks are observed which correspond to the neutron groups that leave the residual nucleus in the ground (n_o), first excited (n_1) and unresolved second and third excited states ($n_2 + n_3$). A small portion of the target gamma rays not rejected by the n/γ discrimination circuit also appear. These serve as a time reference for the determination of the neutron energies.

Laboratory differential cross sections were calculated according to

$$d\sigma/d\Omega = \frac{Y}{Nnd\Omega\varepsilon(E_n)} \qquad (2)$$

where Y is the neutron yield or peak area per total charge integration, N is the number of target nuclei per cm^2, n is the number of deuterons incident on the target per total charge integration, $d\Omega$ is the solid angle subtended by the detector face and $\varepsilon(E_n)$ is the neutron detection efficiency.

4. UNCERTAINTIES IN THE DIFFERENTIAL CROSS SECTIONS

The uncertainties associated with the differential cross sections are as follows:

a) The neutron yield Y contributes 1-13%. This is a statistical error largely associated with the background caused by the tails of neighboring peaks corresponding to other neutron groups which appear in the spectrum.

b) The number of target nuclei per cm^2 N contributes 6-12%. This is a direct consequence of the uncertainties due to non-uniformities in the targets.

c) The number of incident particles per total charge integration n contributes less than about 5%. This is associated with the reliability of the charge integration circuit.

d) Errors in solid angle are less than 1%.

e) The neutron detection efficiency $\varepsilon(E_n)$ contributes about 5-8%. The various origins of this uncertainty have been extensively elaborated in (Na 81).

The totality of the uncertainties from these various parameters results in a overall uncertainty of 7-9% for the differential cross sections at E_d = 7.0 MeV and 9.1 MeV and of 12-18% for those at E_d = 13.0 MeV and for the excitation function at $\theta_{lab} = 25^o$.

5. RESULTS AND ANALYSIS

The experimental center-of-mass differential cross sections are shown in figures 3 and 4. Figure 3 illustrates the excitation curves for the n_o, n_1 and (n_2+n_3) neutron groups at $\theta_{lab} = 25^o$ taken at 200 keV intervals in the range E_d = 10.6 to 13.0 MeV. Figure 4 shows the angular distributions for each of these neutron groups at E_d = 7.0, 9.1 and 13.0 MeV.

a) The Ground State (n_o) Cross Sections

Inspection of the n_o angular distributions reveals a strong direct interaction (stripping) contribution. In addition the excitation curve at $\theta_{lab} = 25^o$ between 10.6 and 13.0 MeV (figure 3) is relatively structureless, as compared with the general behavior of the excitation curve at 0^o obtained by Davis and Din (Da 72) between 3.6 and 12.0 MeV. At the lower energies, the Davis curve is characterized by marked Breit Wigner type resonances which, as the deuteron energy increases, develop into a broad fluctuation pattern reminiscent of the Ericsson fluctuations. In the energy interval considered in the present work we see very little structure since we are at least partially averaging over any fluctuations (ΔE = 100 keV, Γ = 200 keV, D = 70 keV) and thus expect the statistical treatment to be valid. As further insurance, we have adopted the energy averaging techniques of Hodgson (Ho 67), (Ho 71).

To obtain the energy averaged angular distribution at 12.4 MeV, we included the data of Mutchler et al. (Mu 71) at 11.8 MeV. This distribution was normalized to our excitation function at $\theta_{lab} = 25^{o}$. From this borrowed data and our data at 13.0 MeV we obtained the energy averaged differential cross section referred to as the 12.4 MeV angular distribution. From our 7.0 MeV and 9.1 MeV angular distributions we obtained the energy averaged differential cross section referred to as the 8.0 MeV angular distribution.

The direct reaction contribution was obtained from the DWBA stripping analysis at these average energies 8.0 and 12.4 MeV using the computer code DWUCK4 (Ku 74). The optical model potential for calculating the distorted waves in the entrance and exit channels had the form

$$V(r) = V_c(r) - V(1+e^{x})^{-1} + 4iW_D \frac{d}{dx}(1+e^{x_D})^{-1} +$$

$$+ \left(\frac{\hbar}{m_\pi c}\right)^2 \vec{L}.\vec{\sigma} \frac{V_{so}}{r} \frac{d}{dr}(1+e^{x_{so}})^{-1} \qquad (3)$$

where $x = (r-R_o A^{1/3})/a$, $x_D = (r-R_D A^{1/3})/a_D$ and
$x_{so} = (r-R_{so}A^{1/3})/a_{so}$.

The Coulomb potential corresponds to the potential of a uniformly charged sphere of radius $R = R_{oc}A^{1/3}$ ($R_{oc} = 1.3$F). The geometric parameters and strengths of the remaining potentials are given in Table 2. The deuteron parameters were taken from the elastic scattering analysis of Fitz et al. (Fi 67) and the neutron parameters are those of Hodgson et al. (Hod 67). From the local energy approximation, finite range and non-locality corrections were obtained. Non-locality factors of 0.54 F for

the deuteron and 0.85 F for the proton and neutron were used. The finite range correction was $r = 0.65$ F. Partial waves up to $L = 10$ were considered in the calculations.

In the single particle model, the ^{13}N ground state is considered to be a $1p_{1/2}$ proton bound to the ^{12}C core (BE = 1.956 MeV). By fixing this binding energy a potential search executed by the program selected a real well depth of 44.4 MeV for the ^{12}C core. In addition a real Thomas spin orbit term and the Coulomb potential were included.

Adjustments of the various optical parameters for the distorted waves were tested for improvement of fit to the experimental points and those reported in table 2 gave the best results.

No lower cutoffs were used in the DWBA radial integration and a maximum radius of 20 F was maintained. Integration steps of 0.1 F were found to be adequate.

The contribution of the compound nucleus formation was calculated using the Hauser Feshbach computer code of D. Wilmore (Wi 65). This calculates differential cross sections for all the energetically open channels which contribute to the formation and decay of the compound nucleus.

For the incident energies used in this experiment, the continuum in the compound nucleus ^{14}N is not reached and the number of pertinent channels is manageable. Four modes of decay were included in the exit channel: deuteron, neutron, proton and alpha emission. From the reaction thresholds for these various channels, it was found that a total of 18 channels contributed significantly to the compound nucleus decay at $E_d = 8.0$ MeV and 44 channels at $E_d = 12.4$ MeV.

The program requires as input the optical

potentials that describe the channels. These are listed in table 3 for the proton and alpha channels. The deuteron and neutron parameters are the same as those used in the DWBA analysis.

The dependence of the optical parameters on deuteron energy and the width fluctuation correction were found to have little effect on our calculations and for this reason they were not used.

The calculated DWBA (dashed curve) and Hauser Feshbach (dash-point curve) differential cross sections at E_d = 8.0 MeV and 12.4 MeV for the n_o neutron group are shown in figures 5 and 6. The deuteron and neutron optical potentials which were used are those of table 2. Various potential sets were tried, but those of table 2 gave the best overall fits. The experimental values are represented by the points in the figures. The solid curve of figure 5 at E_d = 8.0 MeV was obtained with a direct interaction reduction factor of 0.55 and a Hauser Feshbach factor of 0.40 . The solid curve of figure 6 at E_d = 12.5 MeV was obtained with a direct interaction reduction factor of 0.41 and a Hauser Feshbach reduction factor of 0.40.

b) The First Excited State (n_1) Cross Sections

Angular distributions for the n_1 neutrons at E_d = 7.0 , 9.1 and 13.0 MeV are shown in figure 4 and the excitation function at $\theta_{lab} = 25^o$ from E_d = 10.6 to 13.0 MeV is shown in figure 3. For the n_1 cross sections only the energy averaged angular distribution at 12.4 MeV was used.

The n_1 neutron group leaves the residual nucleus ^{13}N in a state which corresponds to the sharp proton

resonance at 2.365 MeV excitation energy. This state is the unbound mirror of the first excited state of ^{13}C. Application of the DWBA analysis for deuteron stripping to unbound analog states has been investigated by Pessoa and Piza (Pe 81). They conclude that the dominating term in the resonant form factor is the parent state wavefunction. Thus our stripping analysis for the n_1 neutron group consisted of the usual DWBA analysis described earlier but for which the single particle description of the residual nucleus corresponds to the parent state in ^{13}C which is a $2s_{1/2}$ neutron bound by 1.85 MeV to the ^{12}C core.

All the potential sets of optical parameters used for the n_1 analysis are the same as those described in the n_o case. Figure 7 shows the DWBA (dash curve) and the Hauser Feschbach predictions (dash-point curve) for this channel. The solid curve was obtained for a direct interaction reduction factor of 0.28 and a Hauser Feshbach reduction factor of 0.65 .

5. DISCUSSION

The magnitude of our n_o differential cross sections at E_d = 11.8 MeV and $\theta_{cm} = 27.8^o$ is 5.2 mb/sr, Mutchler et al. (Mu 71) reports the value 7.9 mb/sr for this cross section and Davis and Din (Da 72) report a value close to 20 mb/sr at E_d = 12.0 MeV and $\theta_{cm} = 28^o$. Our results seem to agree with those of Shirato (Sh 81) who obtains the value 8 mb/sr for the n_o differential cross section at E_d = 9.1 MeV and $\theta = 0^o$. Although we could not realiably measure the cross section at $\theta = 0^o$ because of the location of the beam stop, extrapolation of our angular distribution at 9.1 MeV indicates

a value of the cross section at 0^o close to 8 mb/sr. For the n_1 differential cross section at E_d = 11.8 MeV and $\theta_{cm} = 28.2^o$ we report the value 3.0 mb/sr as compared to the value 4.8 mb/sr reported by Mutchler et al. (Mu 71).

It should be noted that for both the n_o and n_1 cross sections our values are about 35% lower than those obtained by Mutchler et al. Since theirs is the only other time-of-flight measurement, we later repeated these points and confirmed our original measurements.

For the energy averaged n_o differential cross sections at E_d = 8.0 MeV and E_d = 12.5 MeV, the "best fits" to the experimental points were obtained for a Hauser Feshbach reduction factor, HF = 0.4 . This is smaller than the value HF = 0.58 extracted by Hodgson (Ho 67) from n_o data at E_d = = 2.85 MeV. It is expected, however, that the relative contribution of the direct interaction process should be larger as the deuteron energy increases from 2.85 to 12.4 MeV. This would account for our observed decrease in the compound nucleus factor. Davis and Din (Da 72) assumed the value HF = 0.7 for the Hauser Feshbach reduction factor. They arbitrarily maintained this value throughout their analysis and searched for the "best fit" by varying the optical potentials.

From the "best fits" of figures 5 and 6 we obtained for the direct interaction reduction factor the values DI = 0.55 at E_d = 8.0 MeV and DI = 0.41 at E_d = 12.4 MeV. Since the idea of spectroscopic factor becomes somewhat obscure when competing reaction mechanisms are present, we choose to follow the convention of Hodgson (Ho 67) which considers the direct interaction normalization factor as the equivalent of the spectroscopic factor. The lower value, S = 0.41, which suited

the E_d = 12.4 MeV distribution, agrees well with the value S = 0.38 reported by Azimov (Az 75) for his n_o angular distribution at E_d = 15.25 MeV.

The average energy distribution at E_d = 8.0 MeV presents a rather broad forward peak which would never be fit properly by the predicted DWBA cross section for a transferred proton with L = 1. Davis and Din (Da 72) propose that this behavior suggests that the Hauser Feshbach theory underestimates the magnitude of the compound nuclear component in the reaction mechanism. However, in contrast to their measurements, our backangle behavior follows the predicted stripping pattern which would be impaired if more compound nucleus formation contributed to the reaction mechanism.

The shape of the E_d = 12.4 MeV distribution, with its prominent structure in a region up to $\theta_{cm} = 80^o$, where the cross section is still relatively high, provides more restriction to the choice of spectroscopic factor and the decision of "best fit". For this reason the value S = 0.41 is perhaps the more reliable. This spectroscopic factor differs appreciably from Davis and Din (Da 72) and Mutchler et al. (Mu 71) who reported S = 0.73 and S = 0.74 respectively for the ground state. This is an expected consequence of the difference in the magnitudes of the cross sections for our measurements and those reported by these authors. Our value is, however, lower than the theoretical prediction S = 0.62 of Cohen and Kurath (Co 67) for this state.

For the n_1 neutrons at E_d = 12.4 MeV the "best fit" was obtained for a Hauser Feshbach reduction factor, HF = = 0.65 . This implies that more compound nucleus mechanism contributes to the first excited state than to the ground state.

The spectroscopic factor $S = 0.29$ agrees well with the value $S = 0.25$ reported by Fortune et al. (Fo 69) for the $^{12}C(\tau,d)^{13}N$ data, but is considerably lower than the value $S = 1.02$ reported by Mutchler et al. (Mu 71). For the resonant state description, both of these authors describe the continuum proton by a $2s_{1/2}$ bound-state wave function in ^{13}N calculated for a binding energy of 0.01 MeV.

6. CONCLUSION

Conflicting reports of the n_o differential cross sections for the $^{12}C(d,n)^{13}N$ reaction in the region $E_d = 7.0$ to 13.0 MeV prompted us to investigate this region once again. From the measurements, energy averaged differential cross sections at $E_d = 8.0$ and 12.4 MeV were obtained for the n_o neutrons and at $E_d = 12.4$ MeV for the n_1 neutrons. Analyses of the distributions using optical model, DWBA theory and Hauser Feshbach theory were made. The optical potentials of Fitz et al. (Fi 67) derived from the elastic scattering data was used for the deuteron and of Hodgson (Ho 67) for the neutron. Variations on these potentials were tried in the analyses but it was concluded that the original ones best described the peak positions in the angular distributions. This is a crucial point in extracting the spectroscopic and HF reduction factors since the different sets of optical potentials affected the magnitudes of the predicted distributions at the forward angles by as much as 20%.

The amount of compound nucleus formation persisting at $E_d = 12.4$ MeV is unexpectedly large. This is particularly

true for the n_1 channel which presents a very smooth excitation curve at $\theta_{lab} = 25^o$ between $E_d = 10.6$ and 13 MeV.

The ground state spectroscopic factors are about 30% lower than the theoretical predictions (Co 67) for this state. Part of this is no doubt associated with the liberties in parametrization which the optical model affords.

Although no theoretical estimates of the spectroscopic factor for the first excited state were available, our values agree surprisingly well with the results from the $^{12}C(\tau,d)^{13}N$ data, even though the description of the resonant state form factor is slightly different in the two cases.

ACKNOWLEDGEMENTS

The authors wish to express their thanks to Professor O. Sala for placing the Pelletron facilities at their disposal, the CNPq (Conselho Nacional de Pesquisa) and FINEP for the financial support it provided during this work and Professor V. Toscano of the University of São Paulo Chemistry Department for his help in choosing the target material. One of the authors (H.R.S.) would like to acknowledge the State University of Maringa for the scolarship aid extended to him during this work.

REFERENCES

(As 75) S.A. Azimov et al. Sov. J. Nucl. Physics, Vol. 22, Nº 2, (1975) 1

(Ca 64) E.B. Carter et al. Phys. Rev. 133B (1964) 1421

(Co 67) S. Cohen, D. Kurath Nucl. Phys. A101 (1967) 1

(Da 72) J.R. Davis and G.U. Din Nucl. Phys. A179 (1972) 101

(Fi 67) W. Fitz, R. Jahr and R. Santo Nucl. Phys. A101 (1967) 449

(Fo 69) H.T. Fortune, T.J. Gray, W. Trost and N.R. Fletcher Phys. Rev. 179 (1969) 1033

(Ga 66) A. Gallman et al. Nucl. Phys. 82 (1966) 161

(Ga 70) S. Gangadharan and R.L. Wolke Phys. Rev. C1 (1970) 1333

(Gu 70) H. Guratsch, J. Slotta and G. Stiller Nucl. Phys. A140 (1970) 129

(Ho 67) P.E. Hodgson and D. Wilmore Proc. Phys. Soc. (1967) Vol. 90, 361

(Ho 71) P.E. Hodgson Nuclear Reactions and Nuclear Structure Claredon Press, Oxford (1971)

(Hod 67) P.E. Hodgson Ann. Rev. Nucl. Sci. 17 (1967) 1

(Ku 74) P.D. Kunz DWBA computer code DWUCK4, University of Colorado (1974)

(Mu 71) G. Mutchler, D. Rendic, D.E. Welkley et al. Nucl. Phys. A172 (1971) 469

(Na 81) K. Nakayama, E. Farrelly Pessoa and R.A. Douglas Nucl. Inst. and Methods 190 (1981) 555

(Pe 81) E. Farrelly Pessoa and A.F.R.T. Piza, DWBA analysis for deuteron stripping to analog resonances, Internal Report (1981). (To be published).

(Per 72) C.A. Pearson, J.M. Covan, D. Zisserman et al. Nucl. Phys. A191 (1972) 1

(Pey 74) C.M. Perey and F.G. Perey Atomic Data and Nuclear Data Tables 13 (1974) 293

(Sh 81) S.Shirato Nucl. Inst. and Methods 190 (1981) 29

(Wi 65) D. Wilmore Hauser Feshbach computer code Atomic Energy Research Establishment, Harwell AERE R5053.

(Wy 79) W. Wylie, E.F. Pessoa, E.W. Cybulska, H.R. Schelin, L.M. Fagundes, K. Nakayama and R.A. Douglas Nucl. Inst. and Methods 164 (1979) 293.

TABLE CAPTIONS

TABLE 1 - Charactersitics of the targets used in the present work.

TABLE 2 - Deuteron and neutron optical model parameters used for analysis of the energy averaged differential cross sections at $E_d = 8.0$ MeV and $E_d = 12.4$ MeV.

TABLE 3 - Optical model parameters for the $^{12}C+p$ and the $^{12}C+\alpha$ channels used in the Hauser Feshbach calculation. The parameters for the deuteron and neutron channels are those presented in Table 2.

TABLE 4 - Direct interaction and Hauser Feshbach reduction factors extracted from the analysis of the energy averaged cross sections for the ground and first excited state of ^{13}N.

FIGURE CAPTIONS

FIGURE 1 - Typical neutron time-of-flight spectrum for the $^{12}C(d,n)^{13}N$ reaction at $\theta_{lab} = 30^{o}$ and $E_d = 9.1$ MeV.

FIGURE 2 - Block diagram of the electronics for the neutron time-of-flight detection. Spectroscopy amplifier, AMP; Time pickoff control, TPC; Constant fraction discriminator, CFD; Timing single channel analyser, TSCA; Delay amplifier, DA; Nanosecond delay box, DB; Time to pulse height converter, TAC; Gate and delay generator, GG; Analog to digital converter, ADC.

FIGURE 3 - Excitation function at $\theta_{lab} = 25^{o}$ for the n_o, n_1 and (n_2+n_3) neutron groups.

FIGURE 4 - Angular distributions at $E_d = 7.0$, 9.1 and 13.0 MeV for the n_o, n_1 and (n_2+n_3) neutron groups from the reaction $^{12}C(d,n)^{13}N$. The excitation energy quoted for the unresolved (n_2+n_3) group is the average of the individual excitation energies of the second and third excited states in ^{13}N.

FIGURE 5 - Composition of direct interaction and compound nucleus processes for the $E_d = 8.0$ MeV energy averaged angular distribution of the ground state neutrons. The dashed curve is the DWBA prediction, the dash-point curve is the Hauser Feshbach prediction and the solid curve is the "best fit" to the experimental (solid) points.

FIGURE 6 - Composition of direct interaction and compound nucleus processes for the $E_d = 12.4$ MeV energy averaged angular distribution of the ground state neutrons. The dashed curve is the DWBA prediction, the dash-point curve is the Hauser Feshbach prediction and the solid curve is the "best fit" to the experimental (solid) points.

FIGURE 7 - Composition of direct interaction and compound nucleus processes for $E_d = 12.4$ MeV energy averaged angular distribution of the first excited state neutrons. The dashed curve is the DWBA prediction, the dash-point curve is the Hauser Feshbach prediction and the solid curve is the "best fit" to the experimental (solid) points.

TABLE 1

E_d MeV	thickness (mg/cm^2)	thickness (MeV)	Nº of nuclei of $^{12}C/cm^2$
7.0 9.1	2.02 ± 6.5%	187.67 154.33	9.35×10^{19}
10.0 11.0 12.0 13.0	1.08 ± 11.5%	76.03 70.52 65.77 61.72	5.00×10^{19}

TABLE 2

	V	r_v	a_v	$W=4W_D$	r_w	a_w	$2V_{so}$	r_{so}	a_{so}	r_c	Ref.
deuteron	-118.0	0.887	0.928	24.44	1.52	0.790	-10.0	0.887	0.928	1.3	Fi 67
neutron	-44.8	1.313	0.66	36.76	1.26	0.48	-10.0	1.115	0.57	1.3	Hod 67
proton		1.25	0.65							1.3	

Energies in MeV. Geometrical parameters in F.

TABLE 3

	V	r_v	a_v	$W=4W_D$	r_w	a_w	Ref.
$^{12}C+p$	54	1.25	0.65	28	1.25	0.47	Ga 66
$^{12}C+\alpha$	80	2.07	0.55	16	2.07	0.30	Ca 64

Energies in MeV. Geometrical parameters in F.

TABLE 4

E_d	Residual state	DWBA reduction	Hauser Feshbach reduction
8.0 MeV	^{13}N gs	0.55	0.40
12.4 MeV	^{13}N gs	0.41	0.40
	^{13}N E_x=2.365 MeV	0.29	0.65

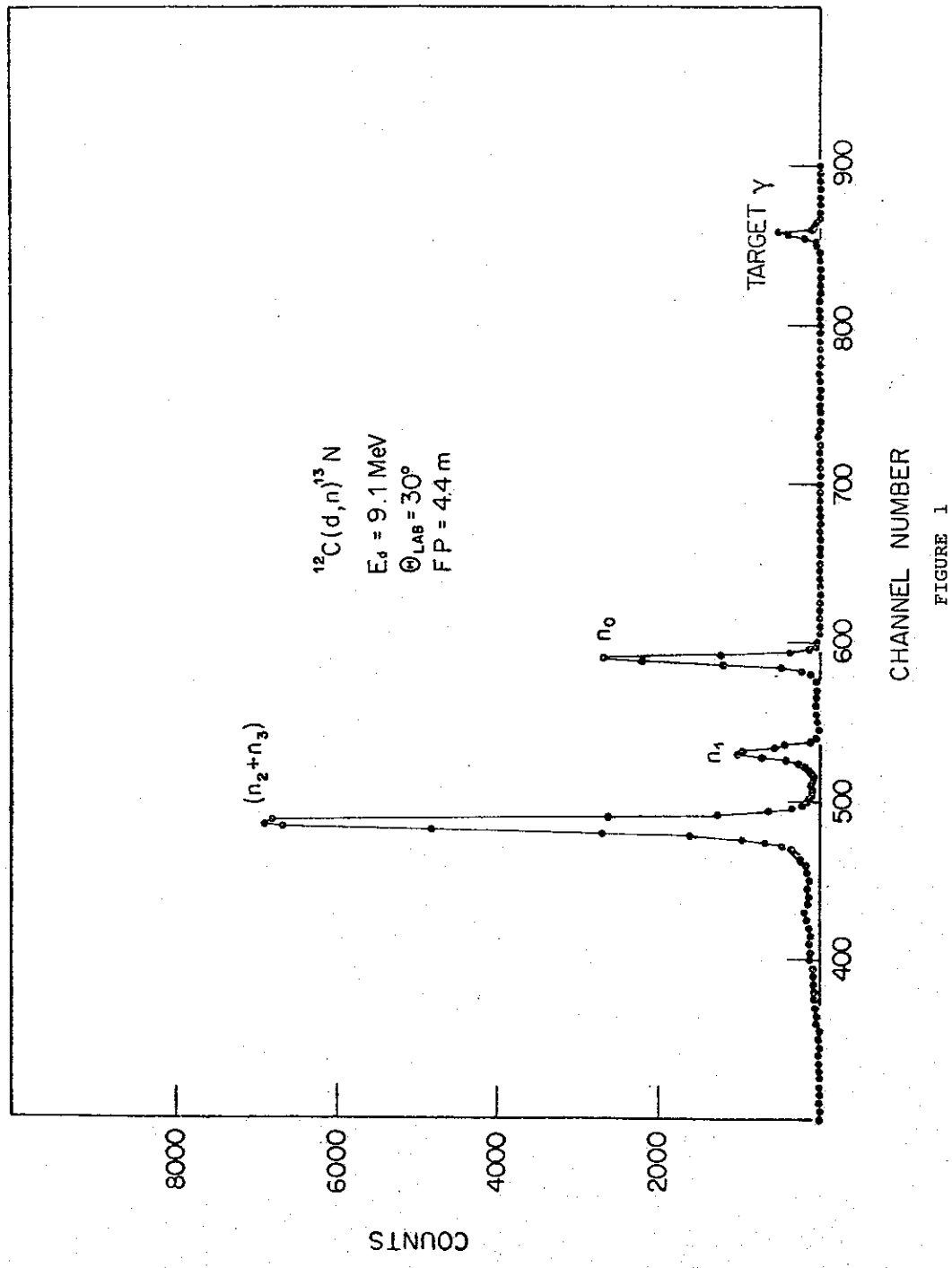

FIGURE 1

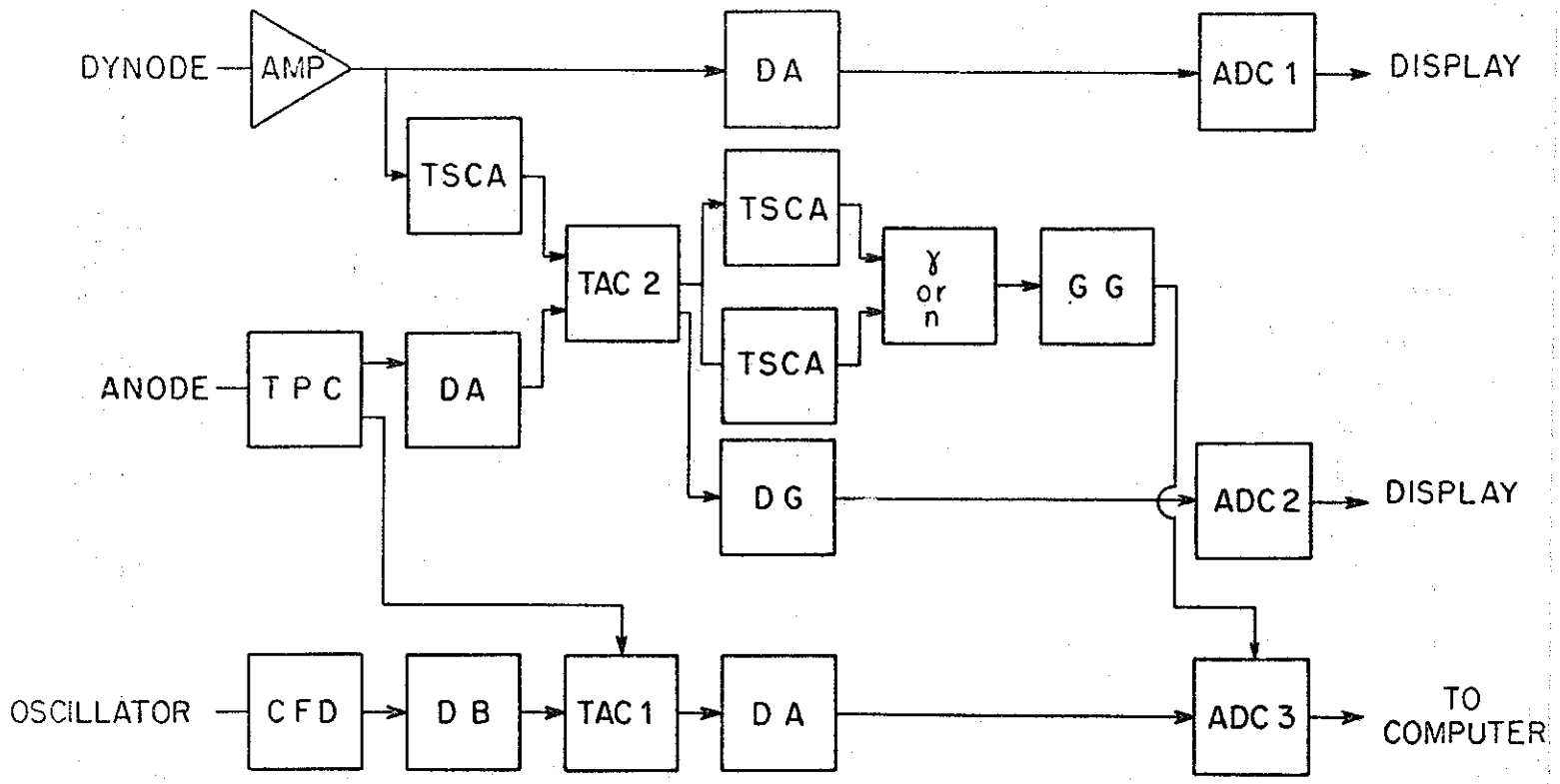

FIGURE 2

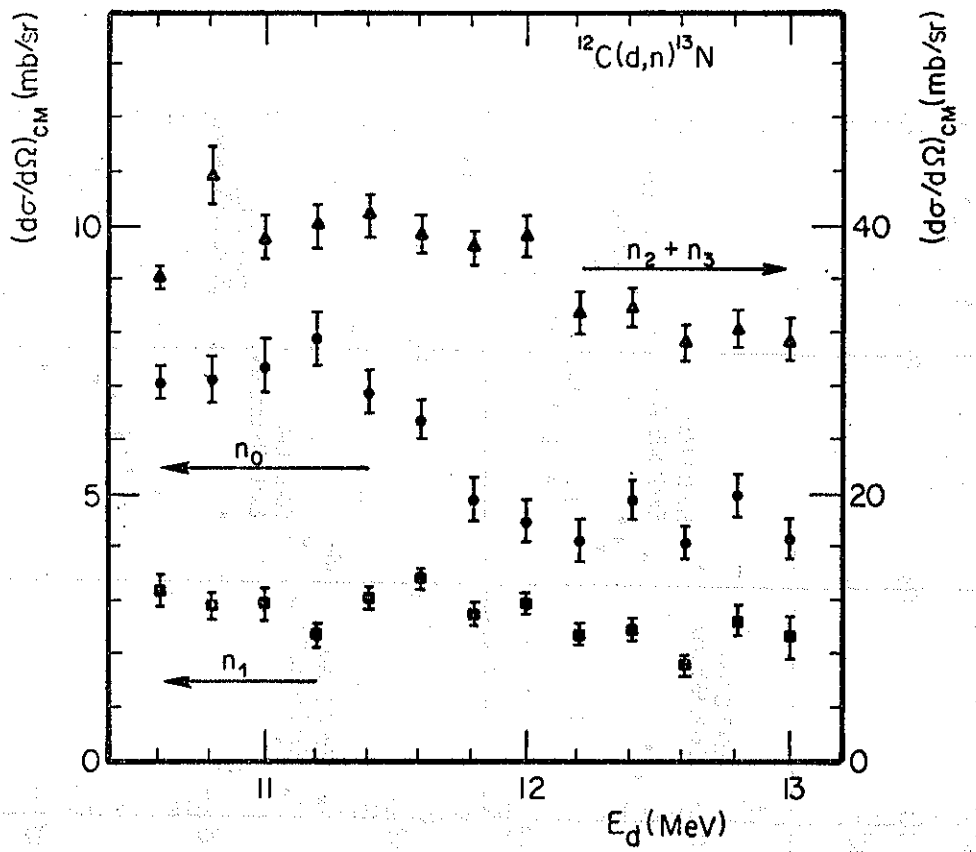

FIGURE 3

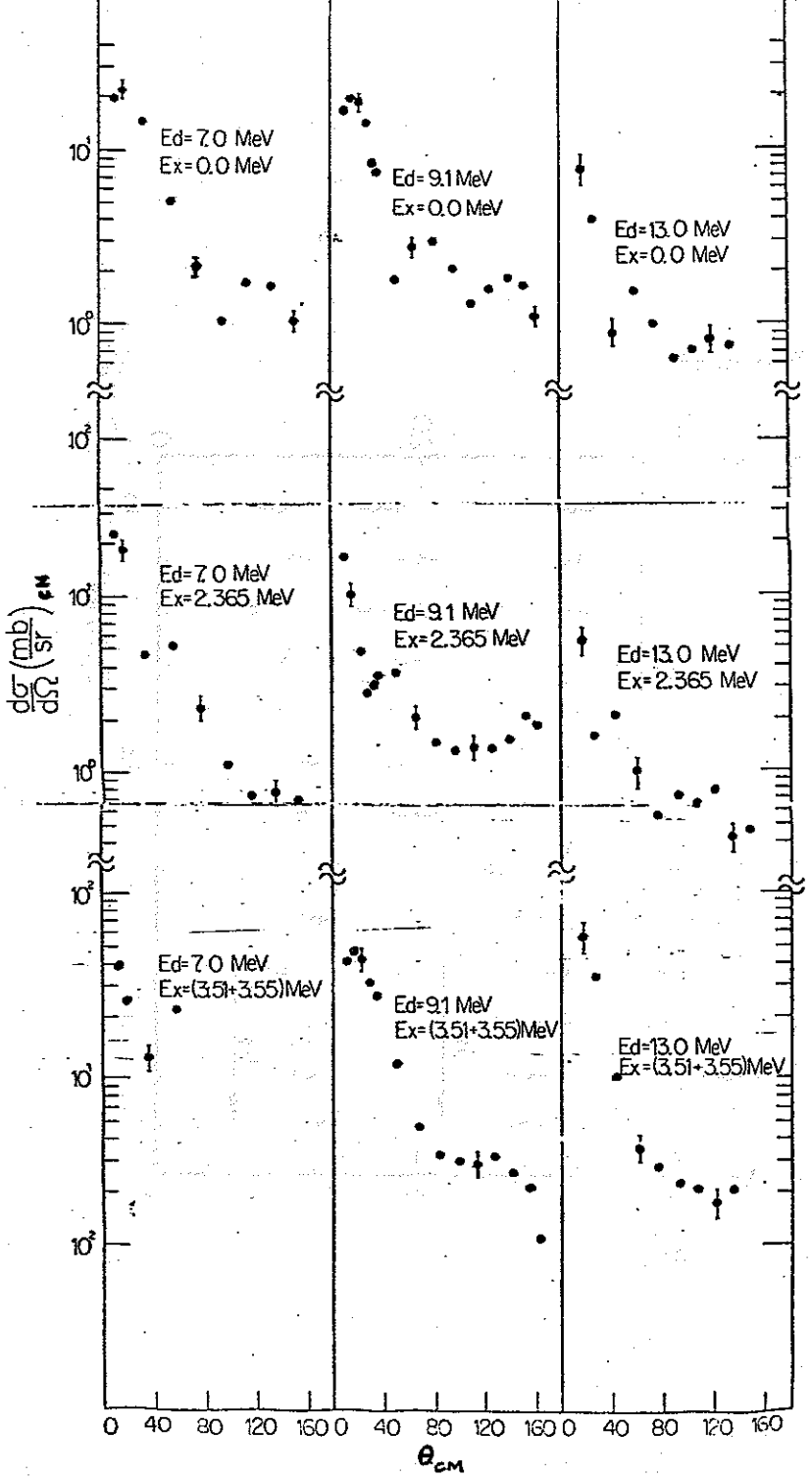

FIGURE 4

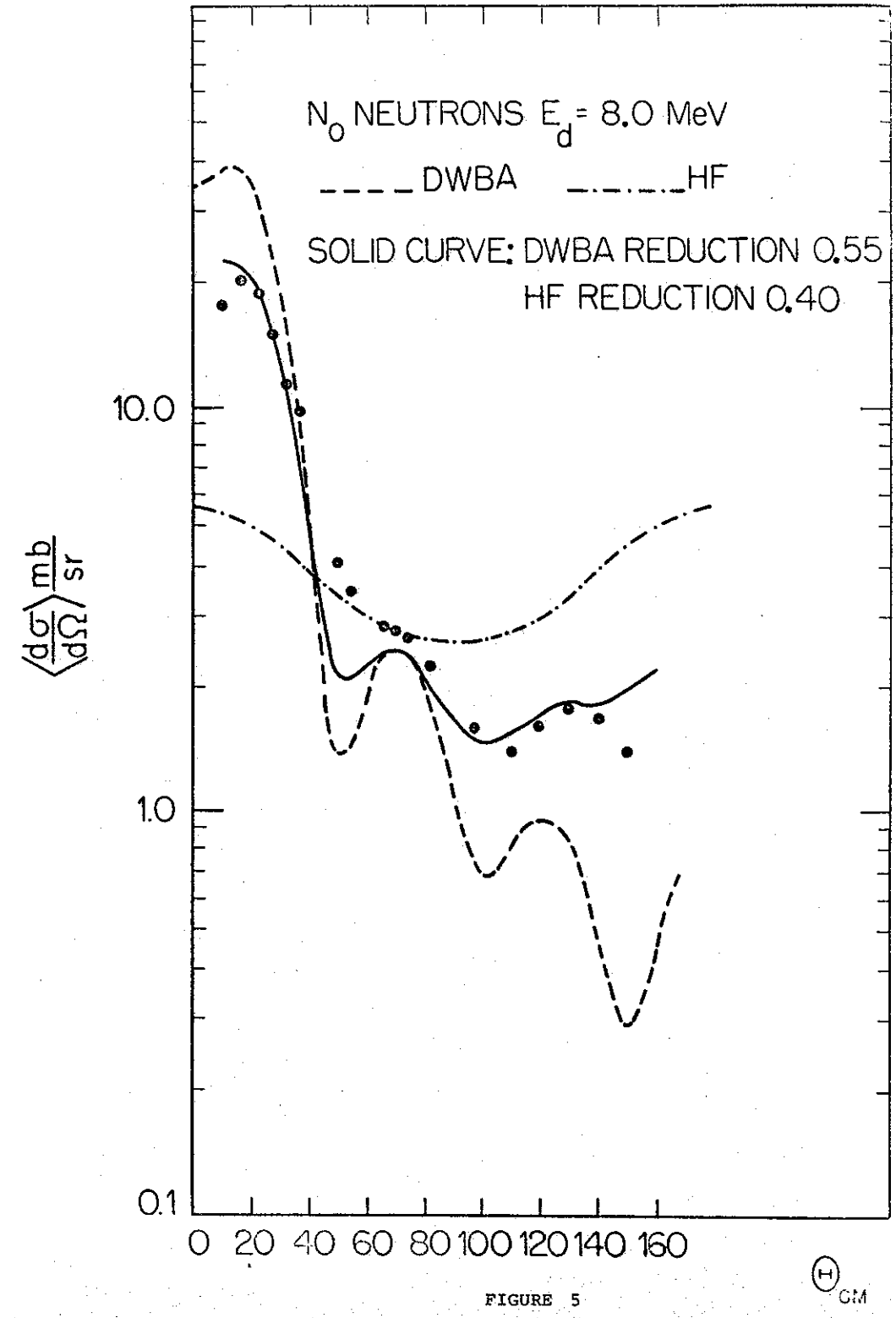

FIGURE 5

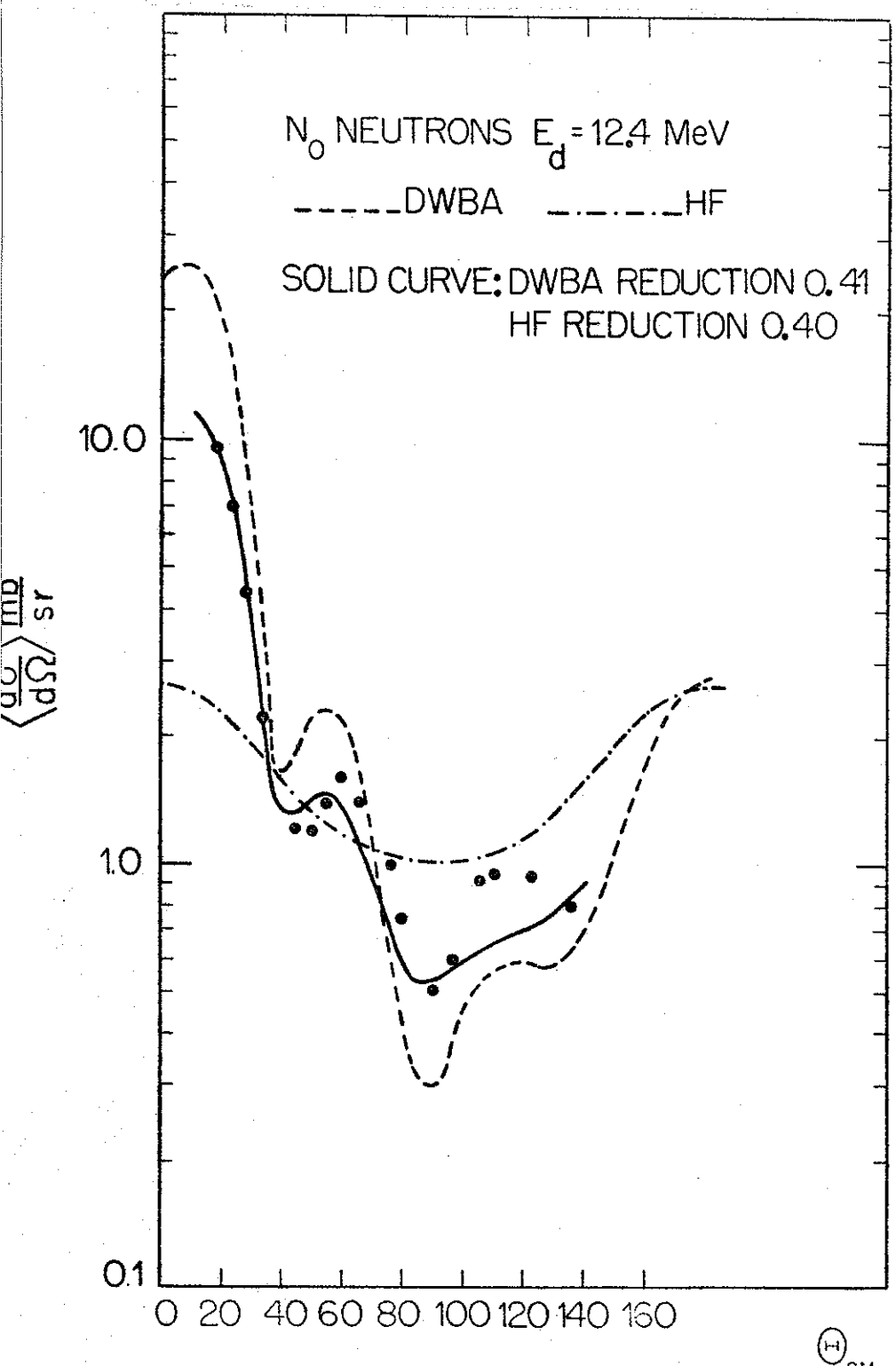

FIGURE 6

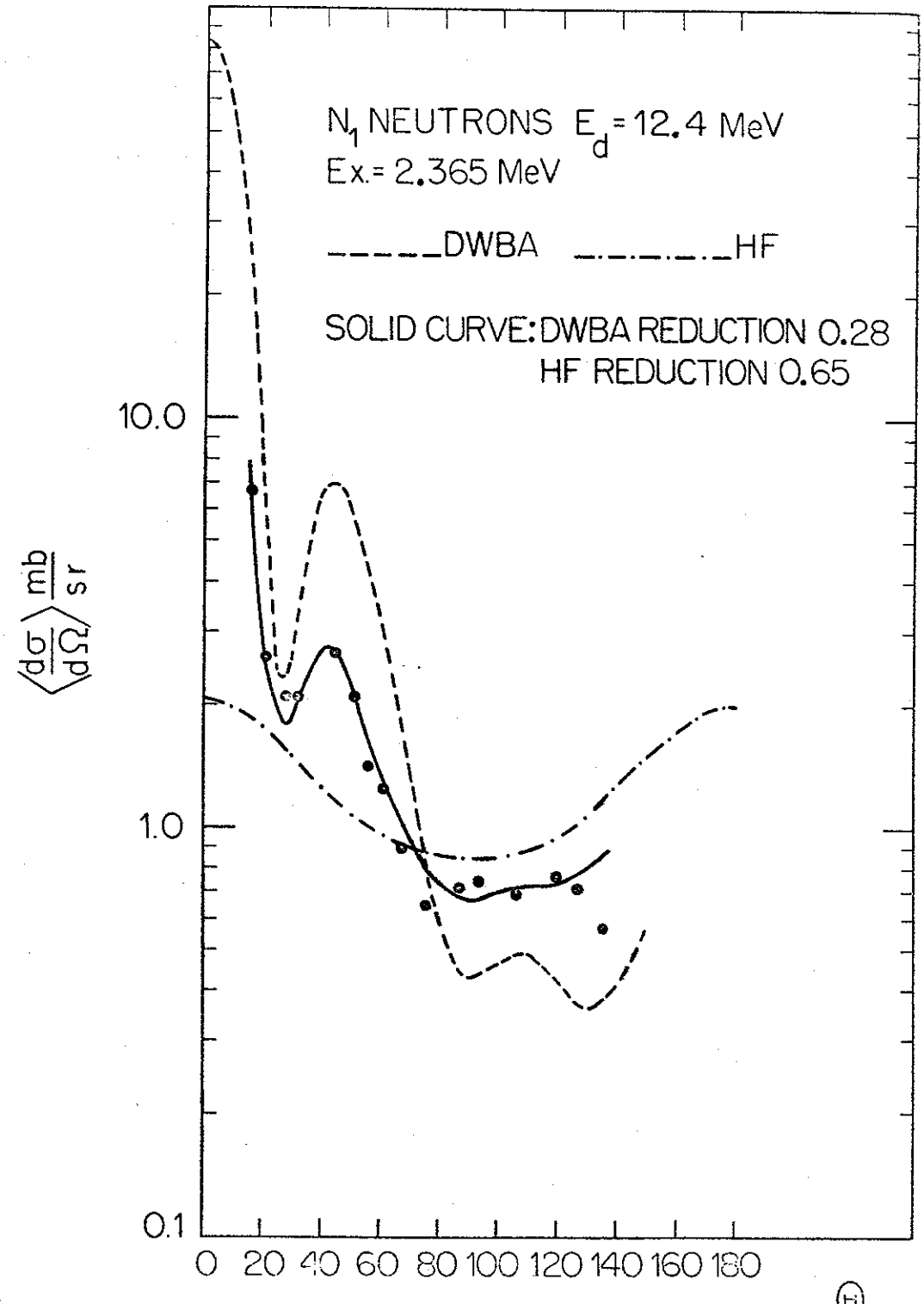

FIGURE 7